IEEE Access
Multidisciplinary | Rapid Review | Open Access Journal

Received November 24, 2021, accepted December 2, 2021, date of publication December 6, 2021,
date of current version December 23, 2021.

Digital Object Identifier 10.1109/ACCESS.2021.3133299

Development of a Low-Cost Modular Structure Fault Tolerant Field Excited Flux Switching Linear Machine for Urban Rail Transit

SHAHID HUSSAIN, (Graduate Student Member, IEEE), FAISAL KHAN, (Member, IEEE), WASIQ ULLAH, (Graduate Student Member, IEEE), BASHARAT ULLAH, (Graduate Student Member, IEEE), AND BAKHTIAR KHAN, (Graduate Student Member, IEEE)

Department of Electrical and Computer Engineering, COMSATS University Islamabad, Abbottabad Campus, Abbottabad 22060, Pakistan

Corresponding author: Wasiq Ullah (wasiqullah014@gmail.com)

This work was supported in part by Comsats University Islamabad, Abbottabad Campus; and in part by the Higher Education Commission of Pakistan under Grant TDF-03-067/R&D/HEC/2019.

ABSTRACT This paper proposes double sided complementary modular field excited flux switching linear machine (FEFSLM). FEFSLM offers the low cost, variable flux capability for a wide speed range, a compact and robust stator which is suitable for the long stroke application. Compared to other linear machines, complementary modular design has more sinusoidal and symmetrical flux linkage and lower detent force. Initially, the topology and machine working principle is thoroughly discussed. To maximize the thrust force of the machine and optimize the geometric parameters, built-in genetic algorithm (GA) of JMAG ver. 20 is utilized. Furthermore, the modular design incorporates the concept of fault-tolerant capabilities to provide the required decoupling between phases. 2D finite element analysis (FEA) is used to analyze the machine performance. Comparatively the optimized design exhibits higher thrust force, lower thrust force ripples and higher efficiency than the initial design.

INDEX TERMS Flux switching machines, linear machines, genetic algorithm, fault tolerant capability.

I. INTRODUCTION

Linear machines have been a popular alternative for urban rail transit systems due to its unique benefit of non-adhesive thrust force. The most notable example is the development and implementation of linear drive machines, which eliminate mechanical friction and produce thrust directly using electromagnetic force, showing great reliability for high speed and efficiency [1], [2]. Linear Induction Machine (LIM) is a conventional linear machine with a simple and robust stator configuration. As a result, LIM has been widely used as a driving motor for railway transit systems such as Guangzhou Metro Line 4 and China's Capital Airport Express Line [3], [4]. For long stroke application, the LIM has the advantages of low cost because there are no windings or magnets on the stator and only the aluminum sheet constitutes the stator, i.e., the rails. However, one of the obvious disadvantages of LIM is that its efficiency and power factor are not satisfactory due to the eddy effect. Presently, linear machines exist of several types in which the most prominent is permanent magnet synchronous linear machine (PMSLM), which has high acceleration and thrust force density. Although, PMSLMs dispersed armature winding (AW) and permanent magnet throughout the primary and secondary components. So, a significant amount of PM or copper is required for long stroke applications [5], [6]. To overcome the problem of the PMSLM, primary permanent magnet linear machines (PPMLM) are investigated in [7]–[9]. In this scenario, the PM flux switching linear machine (PMFSLM) and the PM flux-reversal linear machine (PMFRLM) are regarded breakthroughs in the field of machines and have attracted the attention of many researchers [10]. In PMFSLM both AW and PM are placed in the primary component of these two types of machines, meanwhile the secondary component is constructed entirely of iron [11]. In design of PMFSLM, the excitation part which is primary component act as mover whereas the static secondary part made of iron only is termed as stator due to which preferred for long stoke applications. Since, PM and AW are housed at short mover, this drastically lowered the overall machine cost. However, PPMLM cannot provide

The associate editor coordinating the review of this manuscript and approving it for publication was Paolo Giangrande.

a controllable airgap field, requiring the use of PM, which are expensive and vulnerable to demagnetization.

Furthermore, the switched reluctance machines (SRM) have been investigated for the urban rail transit systems in recent years [10], [12], [13], which comprise of a short primary mover with yokeless iron and armature windings. The advantages of SRM include its simple construction, excellent robustness, and high reliability. SRM has a higher thrust density than LIM, particularly at high speeds and high efficiency and flexible operation for a wide constant power scale. SRM have the disadvantages of high acoustic noise, high thrust force ripples and high vibration [14]. The SRM's application prospects for railway transportation are not promising [15]. Therefore, field excited linear machines take the advantages of low cost and high reliability. A new field excited FRLM based on the magnetic gearing effect has been studied in [16], which not only has the advantages of reduced cost and flux changing capability, but also has better force capability when compared to the conventional. FRLM suffers from the more cogging force and unbalance sinusoidal back electromotive force (EMF). The field excited FSLM is presented in [17], [18] to overcome the aforementioned problems. The proposed machines have the advantages of low cost, reduced mover weight and improve the load capacity. However, based on the literature these types of machines have problem of high-end windings, because these machines adopt the overlapped armature and field windings which have high copper losses and reduce the efficiency of the machines. A new double-sided field excited FSLM with non-overlapped winding has been investigated in [19], [20]. This machine has the merits of low copper losses, high efficiency, larger thrust force, smaller normal force, and better heat dissipation.

Other than machine thrust force, some applications prefers high reliability and fault tolerant capability [21]. The fault-tolerant capabilities of existing machines have been significantly improved by adding alternate poles, introducing modular type design structure, and additional redundant windings in design [22]–[27]. By reducing coupling between phases, a low mutual inductance design may be used to enhance fault-tolerant performance [28], [29]. Meanwhile, to reduce the machines short-circuit current, a design with a high self-inductance can be used [30]. Furthermore, winding configuration in multiphase machines play vital role to enhance fault tolerant capability which make flexibility in control methods. To account, the properties of high fault tolerant performance, low cost and reduced thrust force ripples, this paper presents a double sided complementary modular field excited flux switching linear machine (FEFSLM) with three phase non-overlapped winding.

The rest of this paper is organized as follows, section II presents machine topology and operating principles. Section III investigates the design parameters of the FEFSLM. Detailed electromagnetic analysis based on finite element analysis (FEA) of FEFSLM is examined in section IV. Section V investigates the fault tolerant capability of the proposed machine. Finally, section VI presents the outcome of the study.

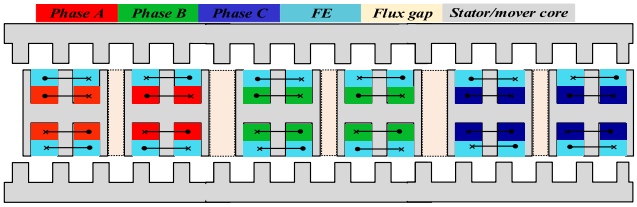

FIGURE 1. Cross sectional view of proposed double sided FEFSLM.

II. MACHINE TOPOLOGY AND OPERATING PRINCIPLE

A. MACHINE TOPOLOGY

Proposed double sided complementary modular FEFSLM topology is shown in Figure. 1. It can be clearly seen that this design does not use any magnets in order to satisfy the requirements of low cost and high reliability. The primary consists of non-overlapped concentrated three phase armature windings and non-overlapped field windings, while the secondary is comprised of salient poles, resulting in a compact and robust construction. The armature windings should be in the same direction, but the field windings should be alternated. Back-to-back E-shaped cores can be seen in each module, whose positions are mutually λ_1 apart, and two consecutive modules combine only one phase.

$$\lambda_1 = \left(i + \frac{1}{2}\right)\tau_s \tag{1}$$

And the displacement between the two adjacent phases can be found by the relation as

$$\lambda_2 = \left(j + \frac{1}{3}\right)\tau_s \tag{2}$$

where i and j are the two positive integers, with values of 2 and 5 respectively and τ_s is the stator pole pitch.

For phase A, coils set A1, A2, A3 and A4 are combined to results more sinusoidal and symmetrical EMF waveforms.

The mover slot in each back-to-back "E" shaped module is divided into two parts. The non-overlapped armature windings are accommodated in the slot towards the mover yoke, and the non-overlapped field windings are adjusted in the slot towards the airgap. Both windings are wound from the mid tooth of the back-to-back "E" shaped module. Between the two modules there is a flux barrier which reduce the mutual inductance and thrust force ripples of the machine. It's worth noting that employing a modular mover design can assist to reduce the amount of detent force. The exploded 3-D view of the proposed machine is shown in Figure. 2.

B. OPERATING PRINCIPLES

The operating principles are based on the no load flux flow generated from a 2D finite element analysis (FEA) using the

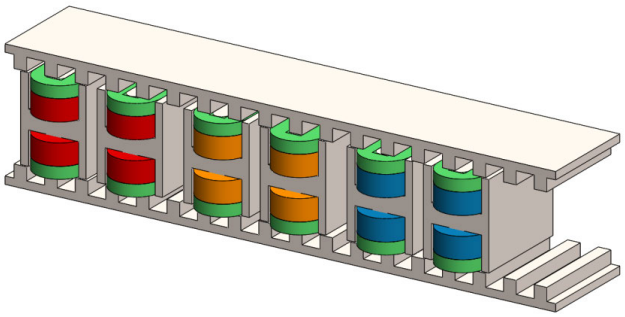

FIGURE 2. 3D view of double sided FEFSLM.

JMAG software (version 20). The flux distribution of the proposed machine follows the two parallel magnetic circuit. The influence of a double-sided field excited coil is addressed, and the flux linkage within a single-phase armature coil is investigated.

Figure. 3(a) displays initial location of the machine at $\theta = 0°$, the flux at that position is maximum positive because the "E" module of coil A1 is aligned with the stator poles. At mover position $\theta = 90°$, the flux of "E" module of coil A1 and "E" module of coil A2 are in the opposite direction, as a result, the net flux flow is zero as shown in Figure. 3(b). In Figure. 3(c), when the mover moves at position $\theta = 180°$, "E" module of coil A2 face the stator poles, which gives the maximum negative flux value. In Figure. 3(d) at mover position $\theta = 270°$, induced flux in the "E" module of coil A1 and "E" module of coil A2 are in opposite directions. As a result, the net flux at that position is nearly equal to zero. Similarly, when the mover moves at one stator pole pitch, coil A1 and coil A2 form a bipolar flux linkage.

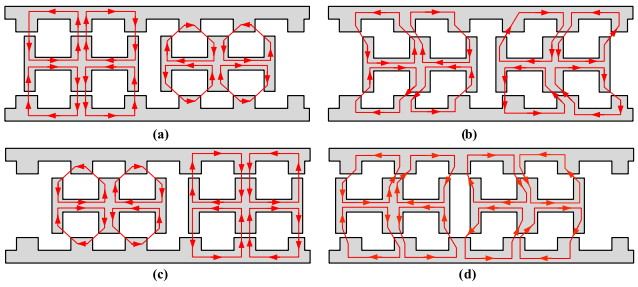

FIGURE 3. Open circuit field distribution at four different mover positions (a) $\theta = 0°$ (b) $\theta = 90°$ (c) $\theta = 180°$ (d) $\theta = 270°$.

III. DESIGN PARAMETER INVESTIGATION

Figure. 4 depicts the geometric parameters of the proposed 12S/14P FEFSLM. The FEFSLM initial parameters are shown in table 1. To achieve globally optimized design parameter for the proposed FEFSLM, FEA based built-in genetic algorithm (GA) of JMAG designer v.20 based multi-variable optimization is performed with the priority to enhance thrust force. It is noteworthy that based on GA, leading design parameters are optimized under fixed constraints

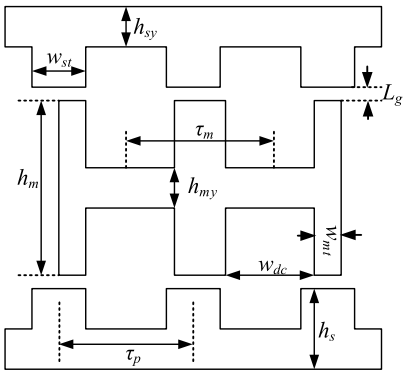

FIGURE 4. Geometric parameters of double sided FEFSLM.

TABLE 1. Initial parameters of double sided FEFSLM.

Symbols	Parameter	Value (Units)
τ_m	Mover pole pitch	77 mm
L_m	Mover stack length	120 mm
w_{mt}	Mover tooth width	10.5 mm
w_{st}	Stator tooth width	11.55 mm
τ_p	Stator pole pitch	36 mm
h_m	Mover height	100 mm
h_{sy}	Stator yoke height	15 mm
w_{dc}	Mover DC slot width	17.5 mm
w_{ac}	Mover armature slot width	17.5 mm
h_{my}	Mover yoke height	20 mm
l_g	Airgap length	1 mm
h_s	Stator height	27 mm
h_{st}	Stator tooth height	12 mm
k_s	Copper filling factor	0.4
V	Rated Velocity	1.5 m/s
I_{rms}	Rated current	6 A

TABLE 2. Fixed outer geometric parameters.

Symbols	Parameter	Value (Units)
τ_m	Mover pole pitch	77 mm
L_m	Mover stack length	120 mm
τ_p	Stator pole pitch	36 mm
h_m	Machine height	156 mm
l_g	Airgap length	1 mm
N_s	Number of mover slots	12
N_p	Number of stator poles	14

of outer design dimension as listed in table 2. Some global optimization variables are mover tooth width (w_{mt}), stator tooth width (w_{st}), mover yoke height (h_{my}), stator yoke height (h_{sy}) and split ratio (k_{sr}).

GA is opted based on boundary conditions (as listed in table. 3), objective function, and constraints as:

TABLE 3. Boundary conditions.

Symbols	Variable	Min.	Max.
h_{my}	Mover yoke	6 mm	35 mm
w_{mt}	Mover tooth width	5 mm	16 mm
w_{st}	Stator pole width	9 mm	17 mm
h_{sy}	Stator yoke height	10 mm	19 mm

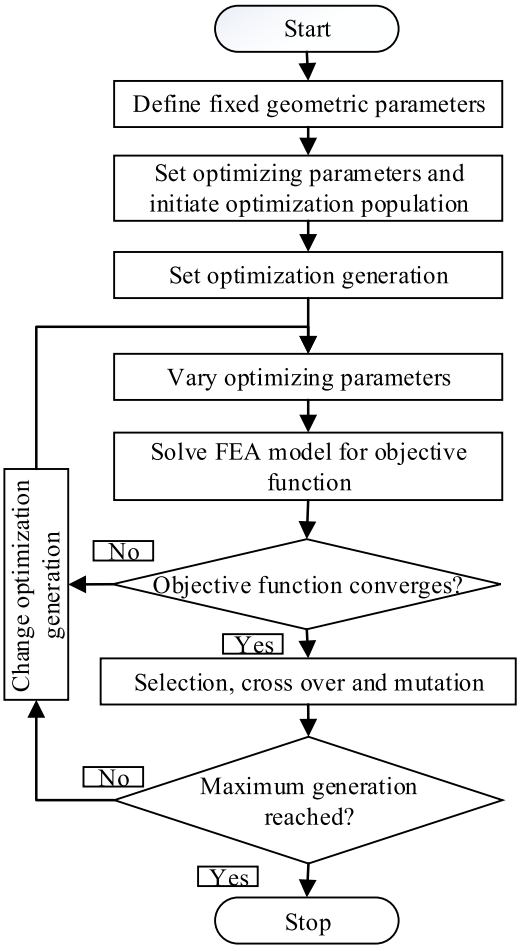

FIGURE 5. Flow chart of the global optimization process.

Objective function

$$max(T.F_{avg})$$

Constraints

$$T.F_{avg} > 681N$$
$$T.F_{ripples} < 12\%$$

Split ratio can be defined as [28]

$$k_{sr} = \frac{h_s + \delta}{h_m + h_s + \delta} \tag{3}$$

where h_s, δ and h_m denotes the stator height, length of airgap and mover heights respectively.

The important geometric parameter in the machine is the mover tooth width which defines the section area of the magnetic flux. Another significant parameter is the mover yoke height, which has a greater impact on the magnetic circuit's loop flux while moving in various directions. In the case of the stator, the width and height of the stator tooth are optimized like mover.

TABLE 4. Optimized parameters of double sided FEFSLM.

Symbols	Parameter	Value (Units)
τ_m	Mover pole pitch	77 mm
L_m	Mover stack length	120 mm
w_{mt}	Mover tooth width	9.1 mm
w_{st}	Stator tooth width	14.93 mm
τ_p	Stator pole pitch	36 mm
h_m	Mover height	100 mm
h_{sy}	Stator yoke height	8.98 mm
w_{dc}	Mover DC slot width	20.33 mm
w_{ac}	Mover armature slot width	20.33 mm
h_{my}	Mover yoke height	22.36 mm
l_g	Airgap length	1 mm
h_s	Stator height	24 mm
h_{st}	Stator tooth height	15.1 mm
k_s	Copper filling factor	0.4
V	Rated Velocity	1.5 m/s
I_{rms}	Rated current	6 A

The flowchart of the global optimization process utilizing GA is shown in Figure. 5. The optimization of the important geometric parameters is done with JMAG's built-in global optimization utilizing the GA method. In the optimization setting, the maximum generation is 20, the population size is 22, number of children is 23 and the stopping criteria is 12. After calculating seven hundred and twenty-two cases with GA, which took almost 192 hours, file size is 26.2 GB and the PC on which optimizing is running is hp core i5, 2.5 GHz, 8GB RAM.

The relationship between the thrust force ripples ratio and thrust force of the double sided FEFSLM with mover yoke, mover pole width, stator pole width and stator yoke are shown in Figure. 6(a-d) respectively. Furthermore, the optimized design exhibits higher thrust force than the initial design. Also, the optimized design shows smaller split ratio than the initial one. The globally optimized parameters of the proposed design are illustrated in table 4.

IV. COMPARATIVE ELECTROMAGNETIC PERFORMANCE

The electromagnetic performances of the initial and optimized FEFSLM including no load flux linkage, back EMF, detent force, airgap flux density and thrust force are investigated.

A. OPEN CIRCUIT FLUX LINKAGE

The open circuit flux linkage of the initial and optimized FEFSLM are shown in Figure. 8(a). As can be observed the Figure shows symmetrical and bipolar waveform because

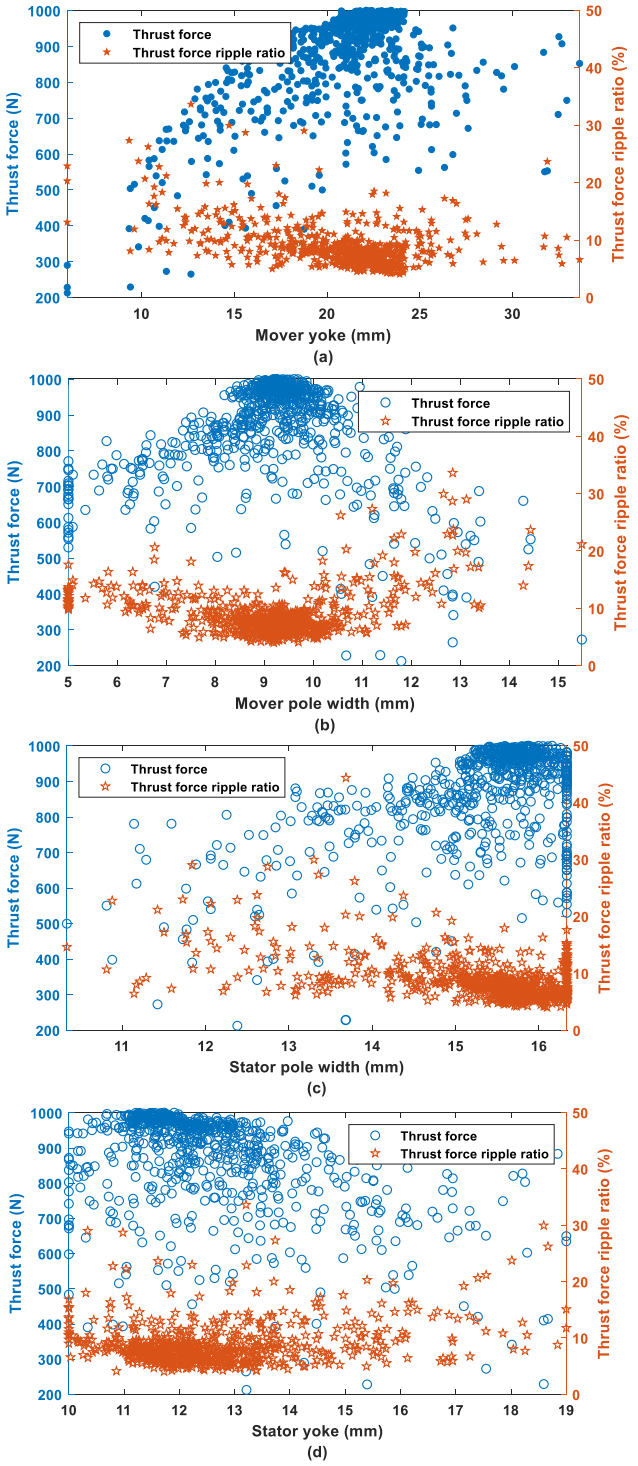

FIGURE 6. Thrust force and thrust force ripple ratio vs (a) Mover yoke (b) Mover pole width (c) Stator pole width and (d) Stator yoke.

there is no influence on end effect due to the complementary modular design. Although, the fundamental amplitude of the optimized design is greater than the initial design. From Figure. 8(b) the third order harmonics have a greater proportion, but have negligible amplitude as compared to the fundamental. However, Figure. 8(b) shows that the higher

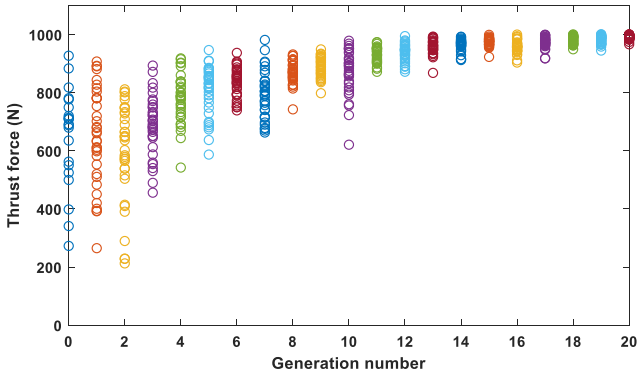

FIGURE 7. Thrust force vs Generation number.

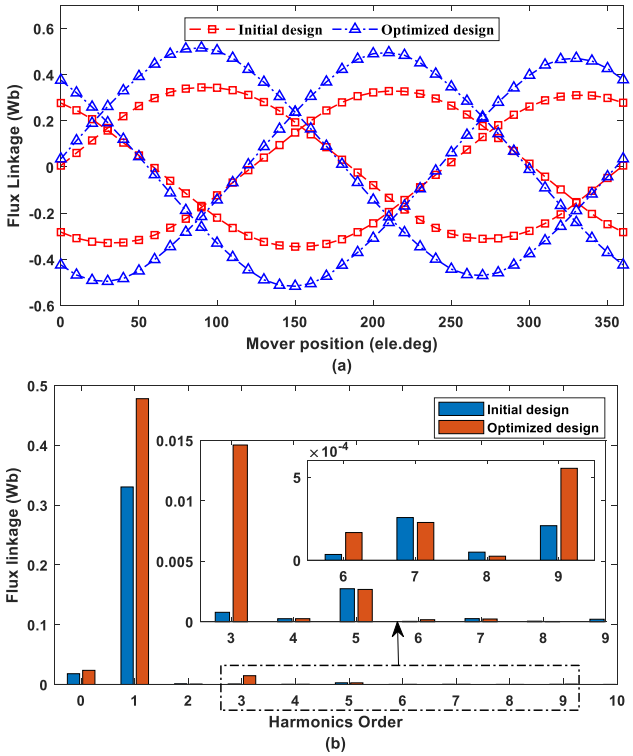

FIGURE 8. Flux linkage (a) waveform (b) Harmonic spectra.

order odd harmonics amplitude of the optimized design is smaller than the initial ones.

B. OPEN CIRCUIT BACK EMF

The open circuit back EMF of the initial and optimized are shown in Figure. 9(a). At the rated velocity of 1.5 m/s both designs offer the sinusoidal and balance three phase back EMF. Furthermore, the optimized design has greater fundamental amplitude as compared to the initial design as shown in Figure. 9(b).

C. FLUX DISTRIBUTION AND FLUX DENSITY

Figure. 10(a) shows the flux distribution of the double sided FEFSLM. The flux density wave form of the initial and

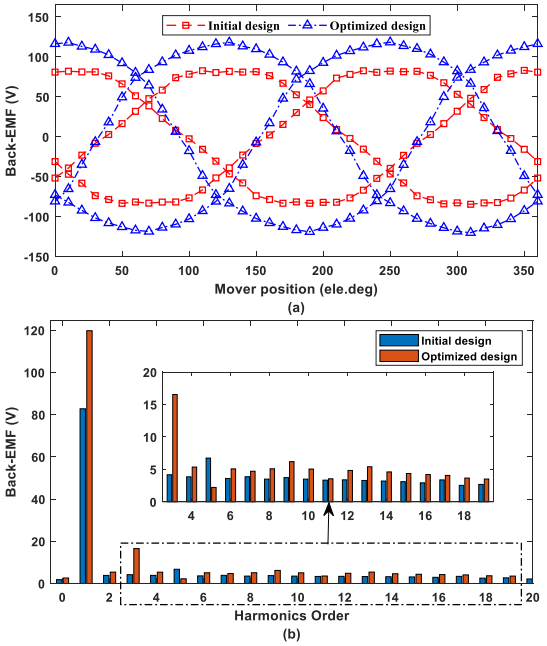

FIGURE 9. Back-EMF (a) waveform (b) Harmonic spectra.

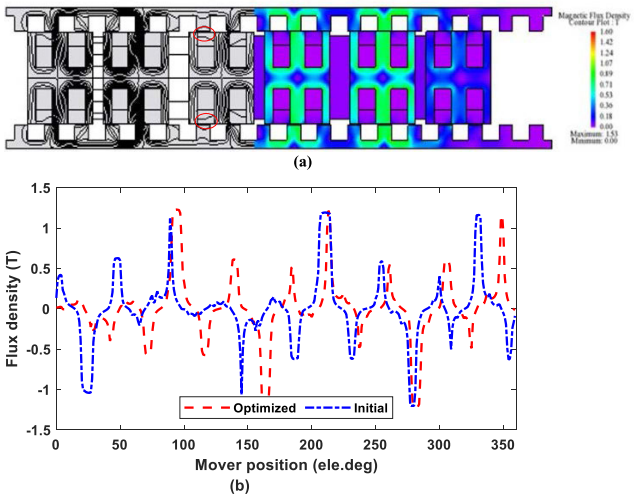

FIGURE 10. (a) No-load flux distribution and (b) No-load air-gap flux density.

optimized design is shown in Figure. 10(b) and can be observed that both designs have quite similar flux density. The flux generated by the field windings mostly passes via the primary yoke, primary teeth, air gap, secondary teeth, and secondary yoke in a sequential order. Despite this, only a small amount of leakage flux passes through the mover slot, which is indicated in red.

D. DETENT FORCE AND THRUST FORCE

As can be seen from Figure. 11(a) that the optimized design exhibit relatively smaller detent force as compared to the initial design. The period of the detent force can be

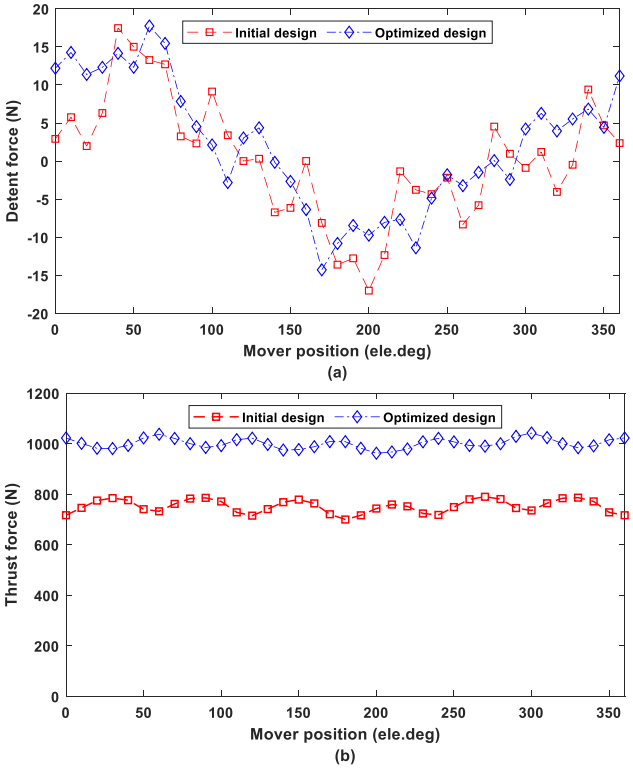

FIGURE 11. (a) Detent force and (b) thrust force.

calculated by

$$N_c = \frac{LCM(N_p, N_s)}{N_s} \tag{4}$$

where N_p and N_s are the pole numbers and slot numbers respectively, while N_c is the number of periods in one electrical cycle. Comparison with other linear machines, the end effect in the complementary modular design is negligible, due to which the detent force in these machines is lower than the other linear machines. However, Figure. 11(b) shows the thrust force waveforms of the initial and optimized designs, and optimized design has 31.91% greater thrust force than the initial.

E. THRUST FORCE RIPPLE RATIO

The thrust force ripple ratio is defined by

$$Ratio = \frac{T.F_{max} - T.F_{min}}{T.F_{avg}} \times 100\% \tag{5}$$

where $T.F_{max}$, $T.F_{min}$, $T.F_{avg}$ are the maximum, minimum and average thrust force values respectively. The variation in the average thrust force of the optimized double sided FEFSLM is shown in Figure. 12(a), while the thrust force ripple ratio is depicted in Figure. 12(b). It can be concluded from Figure. 12 that the thrust force ripple ratio is lowest at the place where the average thrust force value is largest. The optimized design has a ripple ratio of just 7%, whereas the initial design has a ripple ratio of 13%.

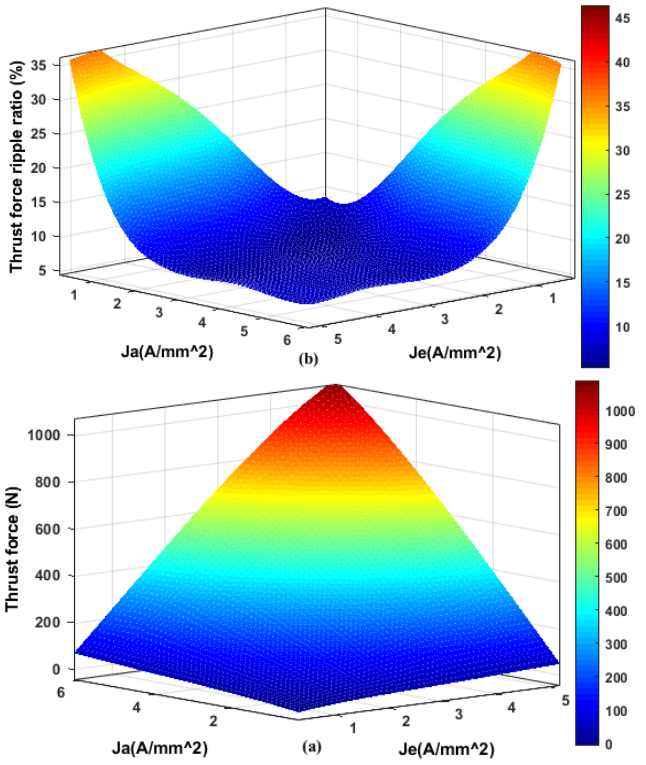

FIGURE 12. (a) Thrust force ripple ratio (b) average thrust force.

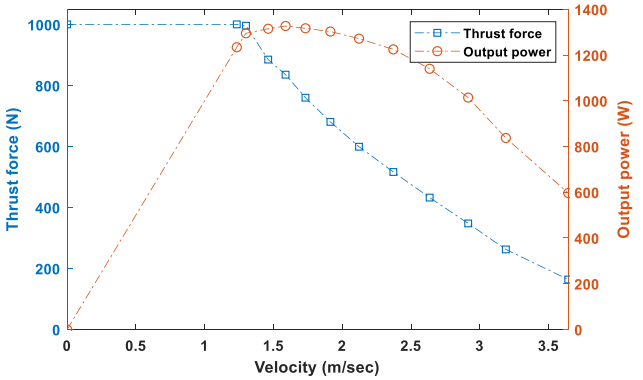

FIGURE 13. Thrust force and output power vs velocity.

TABLE 5. Performance comparision of initial and Optimized design.

Items	Initial	Optimized
No-load flux linkage peak (Wb)	0.345	0.516
Back-EMF peak (V)	82.690	118.356
Detent Force peak (N)	17.733	17.461
Average thrust force (N)	681.193	1001.195
Thrust force ripple ratio (%)	12.115	7.976
Thrust force density $\left({}^{kN}/_{m^3}\right)$	193.081	306.074
Outpower (kw)	1.022	1.326
Efficiency (%)	72.25	76.85

F. CHARACTERISTICS OF THRUST FORCE AND POWER VS VELOCITY

The characteristics of thrust force and power against the velocity for the optimized design is shown in Figure. 13. The maximum output power at the rated velocity is 1326 watt and above rated velocity the power graph is decreasing. Furthermore, at rated velocity the thrust force region is constant, after that the thrust force is dropped to 163.7N at velocity of 3.64 m/sec. Performance comparison of the optimized and initial design are shown in table 5.

V. MATHEMATICAL MODEL OF THE MACHINE

A. MATHEMATICAL MODELLING FOR THREE PHASE SYSTEM

The three-phase flux linkage of the double sided FEFSLM is defined by

$$\begin{cases} \Psi_{ma} = \Psi_0 - \Psi_m \cos(\theta_e) \\ \Psi_{mb} = \Psi_0 - \Psi_m \cos\left(\theta_e - \dfrac{2\pi}{3}\right) \\ \Psi_{mc} = \Psi_0 - \Psi_m \cos\left(\theta_e + \dfrac{2\pi}{3}\right) \end{cases} \tag{6}$$

where Ψ_0 is the DC component and Ψ_m is the fundamental peak amplitude and θ_e denotes the electrical degree of the mover position. The self-inductances and mutual inductances of the machine is expressed as

$$\begin{cases} L_{aa} = L_{dc} + L_m \cos(\theta_e) \\ L_{bb} = L_{dc} + L_m \cos\left(\theta_e - \dfrac{2\pi}{3}\right) \\ L_{cc} = L_{dc} + L_m \cos\left(\theta_e + \dfrac{2\pi}{3}\right) \end{cases} \tag{7}$$

$$\begin{cases} M_{ab} = M_{ba} = M_{dc} + M_m \cos\left(\theta_e - \dfrac{2\pi}{3}\right) \\ M_{bc} = M_{cb} = M_{dc} + M_m \cos(\theta_e) \\ M_{ca} = M_{ac} = M_{dc} + M_m \cos\left(\theta_e + \dfrac{2\pi}{3}\right) \end{cases} \tag{8}$$

where L_{dc} is the DC component and L_m is the fundamental component amplitude of the self inductances while M_{dc} is the DC component and M_m is the findamental component amplitude of the mutual inductance.

By adding flux gaps between adjacent back-to-back "E" shaped modules, which produces a change in the magnetic flux path and the independence between two phases is enhanced. In the mover frame the self-inductances of various phases and mutual inductance of different phases is shown in Figure. 14 and 15 respectively. Due to the physical separation between different phases, it can be observed from the Figure. 14 that the self-inductance is comparatively much more than the mutual inductance. In addition, higher self-inductance reduces short circuit currents in short circuit conditions while lower mutual inductance between different

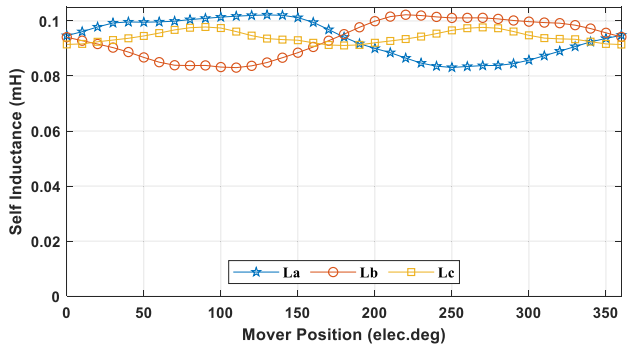

FIGURE 14. Self-inductance.

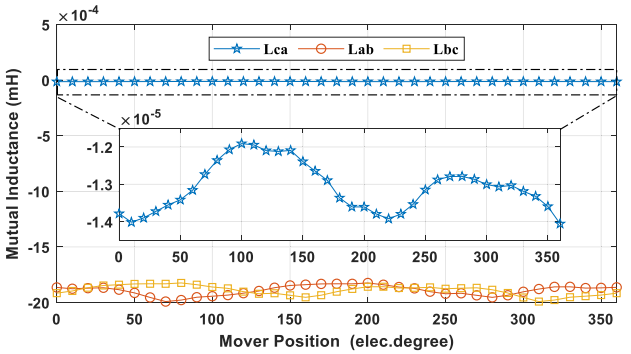

FIGURE 15. Mutual inductance.

phases reduce the interference between the healthy and defective phases.

B. DQ MODELLING IN THE STATOR FRAME

The back EMF and flux linkage waveforms are sinusoidal when the mover of the machine travels over one pole pitch of the stator. As a result, the machine d- and q-axis may be specified as illustrated in Figure. 16, in which the d-axis is that position at which the field flux linkage is at positive maximum, while q-axis is the position where the field flux linkage reaches to zero. The distance between d- and q-axis is 1/4 τ_s.

The dq inductances can be computed through classical park transformation and can be expressed by

$$P = \frac{2}{3}\begin{bmatrix} \cos(\theta_e) & \cos(\theta_e - \frac{2\pi}{3}) & \cos(\theta_e + \frac{2\pi}{3}) \\ -\sin(\theta_e) & -\sin(\theta_e - \frac{2\pi}{3}) & -\sin(\theta_e + \frac{2\pi}{3}) \\ \frac{1}{2} & \frac{1}{2} & \frac{1}{2} \end{bmatrix} \tag{9}$$

The field flux linkage in the form of matrix is expressed as

$$\begin{bmatrix} \Psi_{md} \\ \Psi_{mq} \\ \Psi_{m0} \end{bmatrix} = P \begin{bmatrix} \Psi_{ma} \\ \Psi_{mb} \\ \Psi_{mc} \end{bmatrix} = \begin{bmatrix} -\Psi_m \\ 0 \\ \Psi_0 \end{bmatrix} \tag{10}$$

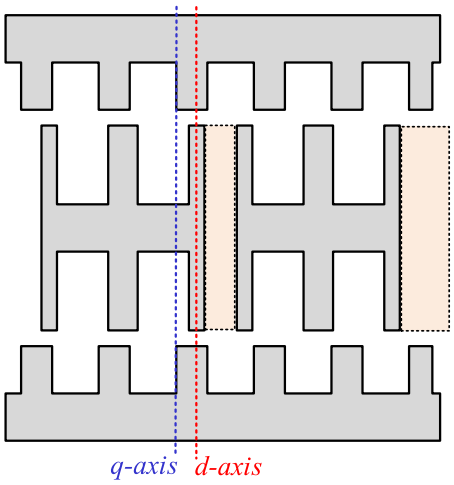

FIGURE 16. Definition of d-and q-axis.

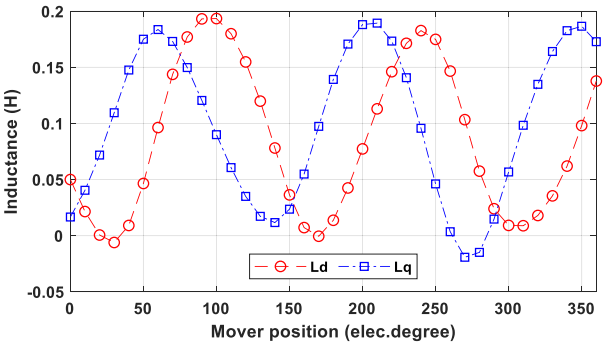

FIGURE 17. dq-axis inductance.

From (10), where d-axis field flux linkage is equal to the fundamental negative peak value of the field flux linkage and q-axis field flux linkage is equal to zero.

The d-q axis inductance can be calculated by the following formula.

$$\begin{bmatrix} L_d & L_{dq} & L_{d0} \\ L_{qd} & L_q & L_{q0} \\ L_{0d} & L_{0q} & L_0 \end{bmatrix} = P \begin{bmatrix} L_{aa} & M_{ab} & M_{ac} \\ M_{ba} & L_{bb} & M_{bc} \\ M_{ca} & M_{cb} & L_{cc} \end{bmatrix} P^{-1} \tag{11}$$

By substituting (7) (8) (9) in (11) we can derive it as

$$\begin{cases} L_d = L_{dc} + \dfrac{L_m \cos(3\theta_e)}{2} \\ L_q = L_{dc} - \dfrac{L_m \cos(3\theta_e)}{2} \\ L_{dq} = -\dfrac{L_m \sin(3\theta_e)}{2} \end{cases} \tag{12}$$

Inductance profile of the proposed FEFSLM along the dq-axis is illustrated in Figure. 17. The resulting generated flux at the adjacent phase winding are 90 degrees apart leading to the least flux interaction between adjacent phase and no mutual flux interaction between end-to-end coils. Therefore, mutual inductance along the dq-axis is usually zero. However, due to

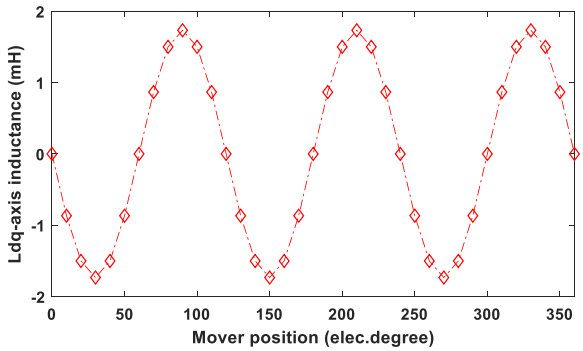

FIGURE 18. dq inductance.

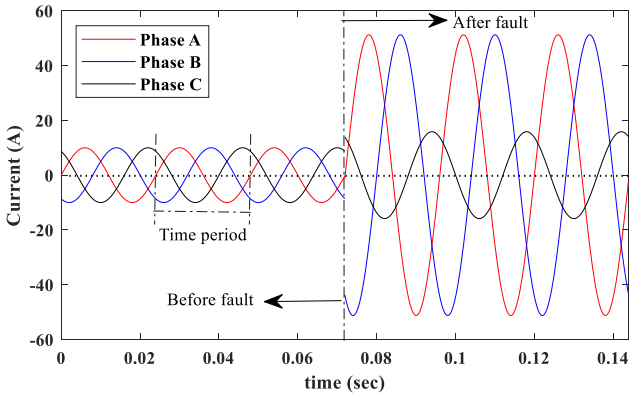

FIGURE 19. Variation of current before and after fault.

variable reluctance flux path in the salient stator and mover teeth, the d and q-axis flux interacts. As a result, mutual inductance along d and q-axis (L_{dq}) is not zero, indicating that the waveform amplitude is small and equals L_{dq} and the waveform is shown in Figure. 18.

C. SHORT CIRCUIT CURRENT

In order to ensure the fault tolerant capability in the proposed machine, the two phases are short circuited through a switch. The current amplitude in the two phases is now higher than the pre-fault condition when the fault occurs at 0.072s (the end of the third electrical period). Figure 19 indicates that the healthy phase has no interdependency with the other two phases during faults, and so the healthy phase has a normal current amplitude before and after faults. As a result, the field excited linear flux switching machine exhibits fault tolerant capability through inductance calculations and short circuit current validation.

VI. CONCLUSION

In this paper a double sided complementary modular FEFSLM has been presented. The machine topology and working principle have been explained in detail. To improve the thrust force and optimize the geometric parameters some global optimization has been implemented on the design. Higher self-inductance and lower mutual inductances were identified in the optimized design, showing that the machine is more fault tolerant. The optimized design had a higher thrust force and reduced thrust force ripples, according to the electromagnetic study. Furthermore, the future work plan is to fabricate the optimized design in order to compare the simulated and experimental results.

APPENDIX

Different types of linear flux switching machines are investigated for urban transit at different scale i.e., as low and high based on mover length, velocity, air-gap length and stack length. At different system specification, the aforesaid parameters widely vary. Therefore, a detailed study on low and high scale design are added in table 6 to highlight variation of the key parameters with the system specification. Based on the design specification, the proposed model is designed at low scale, which can be rescale to large dimension based on the system specification. It is noteworthy that initially models are designed at low scale to save computational time as well as experimental prototype expense.

TABLE 6. Key parameters for urban rail transit.

Reference	Mover Length (mm)	Speed (m/s)	Air gap (mm)	Stack length (mm)	Prototype Scale
[15]	2480	15.68	10	280	high
[27]	504	1.5	2	120	low
[31]	2500	15.68	11	300	high
[32]	504	1.5	1	120	low
[33]	-	30/5	2/0.6	240/80	High/low
[34]	2480	15.68	10	280	high
[35]	504	1.5	1.5	120	low
[36]	384	1.5	1.5	-	low
[37]	551	1.5	1	120	low
[38]	131	4	0.8	90	low

REFERENCES

[1] J. Ji, J. Zhao, W. Zhao, Z. Fang, G. Liu, and Y. Du, "New high force density tubular permanent-magnet motor," *IEEE Trans. Appl. Supercond.*, vol. 24, no. 3, pp. 1–5, Jun. 2014.

[2] J. Wang, D. Howe, and Z. Lin, "Comparative studies on linear motor topologies for reciprocating vapor compressors," in *Proc. IEEE Int. Electr. Mach. Drives Conf.*, May 2007, pp. 364–369.

[3] G. Lv, D. Zeng, T. Zhou, and Z. Liu, "Investigation of forces and secondary losses in linear induction motor with the solid and laminated back iron secondary for metro," *IEEE Trans. Ind. Electron.*, vol. 64, no. 6, pp. 4382–4390, Jun. 2017.

[4] G. Lv, T. Zhou, and D. Zeng, "Influence of the ladder-slit secondary on reducing the edge effect and transverse forces in the linear induction motor," *IEEE Trans. Ind. Electron.*, vol. 65, no. 9, pp. 7516–7525, Sep. 2018.

[5] S.-G. Lee, S.-A. Kim, S. Saha, Y.-W. Zhu, and Y.-H. Cho, "Optimal structure design for minimizing detent force of PMLSM for a ropeless elevator," *IEEE Trans. Mag.*, vol. 50, no. 1, pp. 1–4, Jan. 2014.

[6] M. Ma, L. Li, Z. He, and C. C. Chan, "Influence of longitudinal end-effects on electromagnetic performance of a permanent magnet slotless linear launcher," *IEEE Trans. Plasma Sci.*, vol. 41, no. 5, pp. 1161–1166, May 2013.

[7] L. Xu, W. Zhao, J. Ji, G. Liu, Y. Du, Z. Fang, and L. Mo, "Design and analysis of a new linear hybrid excited flux reversal motor with inset permanent magnets," *IEEE Trans. Magn.*, vol. 50, no. 11, pp. 1–4, Nov. 2014.

[8] R. Cao, C. Mi, and M. Cheng, "Quantitative comparison of flux-switching permanent-magnet motors with interior permanent magnet motor for EV, HEV, and PHEV applications," *IEEE Trans. Magn.*, vol. 48, no. 8, pp. 2374–2384, Aug. 2012.

[9] R. Cao, M. Cheng, and W. Hua, "Investigation and general design principle of a new series of complementary and modular linear FSPM motors," *IEEE Trans. Ind. Electron.*, vol. 60, no. 12, pp. 5436–5446, Dec. 2013.

[10] N. S. Lobo, H. S. Lim, and R. Krishnan, "Comparison of linear switched reluctance machines for vertical propulsion application: Analysis, design, and experimental correlation," *IEEE Trans. Ind. Appl.*, vol. 44, no. 4, pp. 1134–1142, Jul./Aug. 2008.

[11] Q. Tan, M. Wang, and L. Li, "Analysis of a new flux switching permanent magnet linear motor," *IEEE Trans. Magn.*, vol. 57, no. 2, pp. 1–5, Feb. 2021.

[12] T. Hirayama, K. Uwada, and S. Kawabata, "Static characteristics of a double-sided linear switched reluctance motor with high-temperature superconducting excitation winding," in *Proc. 15th Int. Conf. Electr. Mach. Syst. (ICEMS)*, Oct. 2012, pp. 1–4.

[13] H. S. Lim and R. Krishnan, "Ropeless elevator with linear switched reluctance motor drive actuation systems," *IEEE Trans. Ind. Electron.*, vol. 54, no. 4, pp. 2209–2218, Aug. 2007.

[14] Z. Q. Zhu and X. Liu, "Novel stator electrically field excited synchronous machines without rare-earth magnet," in *Proc. 9th Int. Conf. Ecological Vehicles Renew. Energies (EVER)*, Mar. 2014, pp. 1–13.

[15] R. Cao, E. Su, and M. Lu, "Comparative study of permanent magnet assisted linear switched reluctance motor and linear flux switching permanent magnet motor for railway transportation," *IEEE Trans. Appl. Supercond.*, vol. 30, no. 4, pp. 1–5, Jun. 2020.

[16] L. Xu, G. Liu, W. Zhao, J. Ji, H. Zhou, and T. Jiang, "Design and analysis of a new linear wound-field flux reversal machine based on magnetic gear effect," *IEEE Trans. Magn.*, vol. 51, no. 11, pp. 1–4, Nov. 2015.

[17] S. Asfirane, A. Nasr, S. Hlioui, M. Gabsi, O. de La Barriere, Y. Amara, and G. Barakat, "Performance comparison of different winding configurations of a novel wound-field flux-switching linear machine," in *Proc. 13th Int. Conf. Electr. Mach. (ICEM)*, Sep. 2018, pp. 2276–2282.

[18] Y. Jin, R. Cao, Y. Zhang, X. Jiang, and W. Huang, "A new double-sided primary wound field flux-switching linear motor," in *Proc. 18th Int. Conf. Electr. Mach. Syst. (ICEMS)*, Oct. 2015, pp. 243–247.

[19] R. Cao and E. Su, "New double-sided wound field flux-switching linear motor with non-overlapping winding," in *Proc. IEEE Int. Electric Mach. Drives Conf. (IEMDC)*, May 2019, pp. 1746–1751.

[20] N. Ullah, A. Basit, F. Khan, Y. A. Shah, A. Khan, O. Waheed, and A. Usman, "Design and optimization of complementary field excited linear flux switching machine with unequal primary tooth width and segmented secondary," *IEEE Access*, vol. 7, pp. 106359–106371, 2019.

[21] K. Du, W. Zhao, L. Xu, and J. Ji, "Design of a new fault-tolerant linear permanent-magnet Vernier machine," *IEEE J. Emerg. Sel. Topics Ind. Electron.*, vol. 1, no. 2, pp. 172–181, Oct. 2020.

[22] M. J. Jin, C. F. Wang, J. X. Shen, and B. Xia, "A modular permanent-magnet flux-switching linear machine with fault-tolerant capability," *IEEE Trans. Magn.*, vol. 45, no. 8, pp. 3179–3186, Aug. 2009.

[23] R. L. Owen, Z. Q. Zhu, A. S. Thomas, G. W. Jewell, and D. Howe, "Alternate poles wound flux-switching permanent-magnet brushless AC machines," *IEEE Trans. Ind. Appl.*, vol. 46, no. 2, pp. 790–797, Mar./Apr. 2010.

[24] W. Zhao, M. Cheng, W. Hua, H. Jia, and R. Cao, "Back-EMF harmonic analysis and fault-tolerant control of flux-switching permanent-magnet machine with redundancy," *IEEE Trans. Ind. Electron.*, vol. 58, no. 5, pp. 1926–1935, May 2011.

[25] W. Zhao, M. Cheng, J. Ji, R. Cao, Y. Du, and F. Li, "Design and analysis of a new fault-tolerant linear permanent-magnet motor for maglev transportation applications," *IEEE Trans. Appl. Supercond.*, vol. 22, no. 3, Mar. 2012, Art. no. 5200204.

[26] H. Liu, W. Zhao, J. Ji, Y. Du, H. Zhou, and D. Zhang, "Fault-tolerant control of modular linear flux-switching permanent-magnet motor," in *Proc. Int. Conf. Electr. Mach. Syst. (ICEMS)*, Oct. 2013, pp. 1890–1894.

[27] R. Cao, M. Cheng, C. Mi, W. Hua, X. Wang, and W. Zhao, "Modeling of a complementary and modular linear flux-switching permanent magnet motor for urban rail transit applications," *IEEE Trans. Energy Convers.*, vol. 27, no. 2, pp. 489–497, Jun. 2012.

[28] Z. Song, C. Liu, F. Chai, and H. Zhao, "Modular design of an efficient permanent magnet Vernier machine," *IEEE Trans. Magn.*, vol. 56, no. 2, pp. 1–6, Feb. 2020.

[29] Q. Tan, X. Huang, L. Li, and M. Wang, "Magnetic field analysis and flux barrier design for modular permanent magnet linear synchronous motor," *IEEE Trans. Ind. Electron.*, vol. 67, no. 5, pp. 3891–3900, May 2020.

[30] L. Papini, T. Raminosoa, D. Gerada, and C. Gerada, "A high-speed permanent-magnet machine for fault-tolerant drivetrains," *IEEE Trans. Ind. Electron.*, vol. 61, no. 6, pp. 3071–3080, Jun. 2014.

[31] G. Lv, T. Zhou, D. Zeng, and Z. Liu, "Design of ladder-slit secondaries and performance improvement of linear induction motors for urban rail transit," *IEEE Trans. Ind. Electron.*, vol. 65, no. 2, pp. 1187–1195, Feb. 2018.

[32] R. Cao, E. Su, and M. Lu, "Comparative study of permanent magnet assisted linear switched reluctance motor and linear flux switching permanent magnet motor for railway transportation," *IEEE Trans. Appl. Supercond.*, vol. 30, no. 4, pp. 1–5, Jun. 2020.

[33] R. Cao, M. Cheng, and B. Zhang, "Speed control of complementary and modular linear flux-switching permanent-magnet motor," *IEEE Trans. Ind. Electron.*, vol. 62, no. 7, pp. 4056–4064, Jul. 2015.

[34] R. Cao, Y. Jin, Z. Zhang, and M. Cheng, "A new double-sided linear flux-switching permanent magnet motor with yokeless mover for electromagnetic launch system," *IEEE Trans. Energy Convers.*, vol. 34, no. 2, pp. 680–690, Jun. 2019.

[35] R. Cao, M. Lu, N. Jiang, and M. Cheng, "Comparison between linear induction motor and linear flux-switching permanent-magnet motor for railway transportation," *IEEE Trans. Ind. Electron.*, vol. 66, no. 12, pp. 9394–9405, Dec. 2019.

[36] R. Cao, M. Cheng, C. Mi, W. Hua, and W. Zhao, "A hybrid excitation flux-switching permanent magnet linear motor for urban rail transit," in *Proc. IEEE Vehicle Power Propuls. Conf.*, Sep. 2011, pp. 1–5.

[37] W. Hao and Y. Wang, "Analysis of double-sided sandwiched linear flux-switching permanent-magnet machines with staggered stator teeth for urban rail transit," *IET Electr. Syst. Transp.*, vol. 8, no. 3, pp. 175–181, Sep. 2018.

[38] B. Ullah, F. Khan, A. H. Milyani, N. Ahmad, and K. M. Cheema, "Design and analysis of dual-stator hybrid excited linear flux switching machine for long-stroke applications," *IET Electr. Power Appl.*, vol. 15, no. 12, pp. 1678–1691, Dec. 2021.

SHAHID HUSSAIN (Graduate Student Member, IEEE) was born in Swabi, Khyber Pakhtunkhwa, Pakistan. He received the B.S. degree in electrical power engineering from COMSATS University Islamabad, Abbottabad Campus, Abbottabad, Pakistan, in 2019, where he is currently pursuing the M.S. degree in electrical power engineering. Since 2020, he has been a Research Assistant with the Machine Design Group. His research interests include design analysis, optimization, and experimental validation of modular and complementary fault tolerant field excited linear flux switching machines for long stroke application. He is a member of Pakistan Engineering Council.

FAISAL KHAN (Member, IEEE) was born in Charsadda, Khyber Pakhtunkhwa, Pakistan, in 1986. He received the B.S. degree in electronics engineering and the M.S. degree in electrical engineering from COMSATS University Islamabad (Abbottabad Campus), Pakistan, in 2009 and 2012, respectively, and the Ph.D. degree in electrical engineering from Universiti Tun Hussein Onn Malaysia, Malaysia, in 2017.

From 2010 to 2012, he was a Lecturer at the University of Engineering and Technology, Abbottabad, Pakistan. Since 2017, he has been an Assistant Professor with the Electrical and Computer Engineering Department, COMSATS University Islamabad (Abbottabad Campus). He is the author of more than 100 publications and one patent. His research interests include design and analysis of flux-switching machines, synchronous machines, and DC machines.

Dr. Khan is a member of IEEE-IES Electrical Machines Technical Committee. He received multiple research awards.

WASIQ ULLAH (Graduate Student Member, IEEE) was born in Peshawar, Khyber Pakhtunkhwa, Pakistan, in 1995. He received the B.S. and M.S. degrees in electrical (power) engineering from COMSATS University Islamabad (Abbottabad Campus), Abbottabad, Pakistan, in 2018 and 2020, respectively, where he is currently pursuing the Ph.D. degree in electrical (power) engineering.

Since 2018, he has been a Research Associate with the Electric Machine Design Research Group. His research interests include analytical modeling, design analysis and optimization of permanent magnet flux switching machines, linear flux switching machines, hybrid excited flux switching machines, and novel consequent pole flux switching machines for high-speed brushless AC applications.

Mr. Ullah serve as a Reviewer for IEEE Access and *IET Electric Power Application*. He is a member of IEEE-IES and Pakistan Engineering Council.

BASHARAT ULLAH (Graduate Student Member, IEEE) received the B.Sc. degree in electronics engineering from the University of Engineering and Technology (UET), Peshawar, Pakistan, in 2015, and the master's degree in power electronics and control systems from the National University of Sciences and Technology (NUST), Islamabad, Pakistan, in 2017. He is currently pursuing the Ph.D. degree in electrical engineering with COMSATS University Islamabad. His research interests include design of flux-switching machines, drives for AC/DC rotary and linear machines, optimal control, and switched mode power supplies, including model predictive control of power electronic dc-dc converters.

BAKHTIAR KHAN (Graduate Student Member, IEEE) received the B.Sc. degree in electrical engineering from the University of Engineering and Technology, Peshawar, Pakistan, in 2007, and the M.Sc. degree in electrical engineering from COMSATS University Islamabad (CUI), Abbottabad Campus, Pakistan, in 2018, where he is currently pursuing the Ph.D. degree in electrical engineering. His research interest includes design and analysis flux switching machines (FSMs) and synchronous machines for high-speed applications. He is a member of the Pakistan Engineering Council.